Granular PEG hydrogels mediate osteoporotic MSC clustering via N-cadherin influencing the pro-resorptive bias of their secretory profile

Varsha V. Rao[1,2], **Marissa E. Wechsler**[3], **Emily Cravens**[4], **Samantha J. Wojda**[4], **Alexander S. Caldwell**[1,2], **Bruce E. Kirkpatrick**[1,2,5], **Seth W. Donahue**[4], **Kristi S. Anseth**[1,2,*]

[1.]Department of Chemical and Biological Engineering, University of Colorado – Boulder 3415 Colorado Avenue, Boulder, CO 80303, USA

[2.]BioFrontiers Institute, University of Colorado – Boulder 3415 Colorado Avenue, Boulder, CO 80303, USA

[3.]Department of Biomedical Engineering and Chemical Engineering, University of Texas San Antonio, One UTSA Circle, San Antonio, TX 78249, USA

[4.]Department of Biomedical Engineering, University of Massachusetts Amherst, 240 Thatcher Road, Amherst, MA 01003

[5.]Medical Scientist Training Program, University of Colorado Anschutz Medical Campus 13001 East 17th Aurora, CO 80045, USA

Abstract

Postmenopausal osteoporosis results from a pro-resorptive bone environment, which decreases bone mineral density and increases fracture risk. Bone marrow derived mesenchymal stem/stromal cells (MSCs) secrete factors involved in bone homeostasis, but osteoporosis mediated changes to their secretions remain understudied. Herein, we examined the secretome of MSCs isolated from ovariectomized rats (OVX rMSCs), a model of post-menopausal osteoporosis, as a function of cell-cell interactions. Specifically, we controlled clustering of OVX and SHAM rMSCs by assembling them in granular hydrogels synthesized from poly(ethylene glycol) microgels with average diameters of ~10, 100, and 200 μm. We directed both the size of rMSC clusters (single cells to ~30 cells/cluster) and the percentages of cells within clusters (~20-90%) by controlling the scaffold pore dimensions. Large clusters of OVX rMSCs had a pro-resorptive secretory profile, with increased concentrations of Activin A, CXCL1, CX3CL1, MCP-1, TIMP-1, and TNF-α, compared to SHAM rMSCs. As this pro-resorptive bias was only observed in large cell clusters, we characterized the expression of several cadherins, mediators of cell-cell contacts. N-cadherin

expression was elevated (~4-fold) in OVX relative to SHAM rMSCs, in both cell clusters and single cells. Finally, TIMP-1 and MCP-1 secretion was only decreased in large cell clusters of OVX rMSCs when N-cadherin interactions were blocked, highlighting the dependence of OVX rMSC secretion of pro-resorptive cytokines on N-cadherin mediated cell-cell contacts. Further elucidation of the N-cadherin mediated osteoporotic MSC secretome may have implications for developing therapies for postmenopausal osteoporosis.

Graphical Abstract
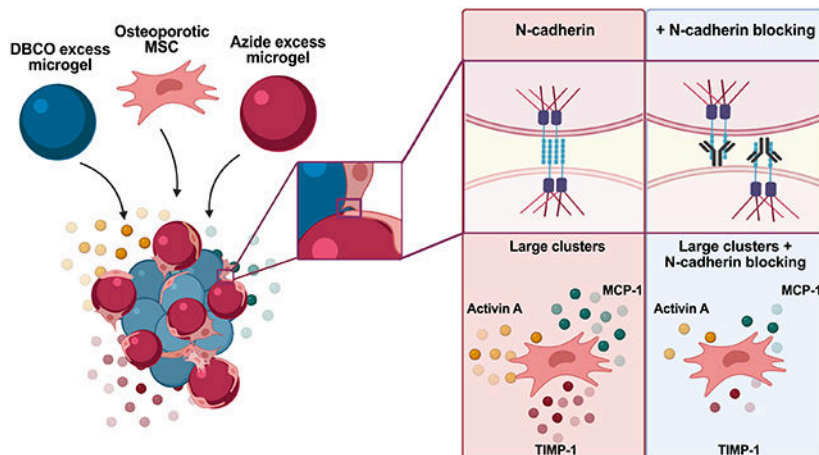
Keywords

N-cadherin; MSC secretome; porous scaffolds; granular hydrogels; osteoporosis; ovariectomy (OVX)

1 INTRODUCTION

Initiated by estrogen deficiency during menopause, Type 1 or postmenopausal osteoporosis (OP) is a bone disorder that affects tens of millions of women worldwide[1,2]. OP is characterized by decreased bone mineral density and increase bone marrow adiposity, leading to bone fragility and increased fracture risk[2,3]. The loss of bone mass is a result of an imbalanced rate of bone turnover, where the rate of bone resorption outpaces the rate of bone formation. The main cell types involved in the bone turnover processes are osteoclasts, responsible for bone resorption, and osteoblasts, responsible for bone matrix deposition. In OP, the loss of estrogen leads to increased pro-inflammatory signaling, osteoclast fusion, and osteoblast apoptosis, collectively leading to a pro-resorptive bone marrow environment.

Bone marrow derived mesenchymal stem/stromal cells (MSCs) are a heterogenous population of multipotent and secretory cells involved in bone homeostasis, osteoporosis, and fracture healing [4-6]. In healthy environments, a subset of MSCs differentiate primarily into osteoblasts and to a lesser extent into adipocytes. However, MSCs isolated from osteoporotic environments, specifically from ovariectomized rats (OVX rMSCs), have decreased osteogenic capacity and are biased towards adipogenesis *in vitro* [7,8]. Beyond their differentiation potential, MSCs secrete a variety of factors—including cytokines,

growth factors, and chemokines—that influence bone remodeling. MSCs secrete factors that can direct osteoblast differentiation and matrix deposition, osteoclast fusion and resorption activity, and macrophage and lymphocyte migration and polarization, all functions that directly impact osteoporosis[5,9]. While normal bone resorption/formation balance is known to be impaired in osteoporosis, less is known about how the secretome of osteoporotic MSCs may be changed or how these changes might influence bone remodeling.

Prior work has determined that MSC secretory properties are dependent on their *in vitro* culture microenvironments [10-13]. In previous studies, OVX rMSCs have been cultured on tissue culture polystyrene (TCPS); however, TCPS culture and expansion can adversely affect MSC secretory properties [14]. Alternative culture systems have evolved to address this problem. For example, systems that promote MSCs cellular interactions, such as spheroid culture [15,16] and porous scaffolds [14,17,18], are known to promote MSC secretions, in part through N-cadherin signaling[14,17,18]. Granular porous scaffolds can be particularly advantageous as a they require a fewer number of cells and maintain a high degree of cell-matrix interactions. However, the influence of N-cadherin mediated cell-cell contacts on the OVX rMSC secretome is not fully understood.

Herein, we used porous granular hydrogels to tailor the clustering OVX rMSCs in order to study their secretome. OVX rMSCs were isolated from ovariectomized rats exhibiting osteoporotic bone parameters, including decreased bone mineral density and volume. To control rMSC clustering, poly(ethylene glycol) based granular hydrogel scaffolds were synthesized from micrometer-sized hydrogel spheres (diameters ~10, 100, and 200 μm), termed microgels. Trophic factors secreted from OVX and SHAM control rMSCs were measured as a function of cell clustering and cluster size. In large clusters, we observed increased secretion of pro-resorptive and anti-osteogenic factors by OVX relative to SHAM rMSCs. For this reason, we investigated the gene expression of cadherin molecules (facilitators of cell-cell contacts) in OVX and SHAM rMSCs. Further, we block cadherin signaling and investigate downstream effects on the secretory properties of OVX and SHAM rMSCs. The reported results suggest that differences in the OVX rMSC secretory profile are influenced by cadherin expression and binding, which may contribute to the overall pro-resorptive nature of the osteoporotic bone environment.

2 MATERIALS AND METHODS

2.1 Ovariectomy surgery and subsequent trabecular bone characterization

All animal experiments were completed in accordance with National Institutes of Health guide for the care and use of laboratory animals and with approval from the University of Massachusetts institutional animal care and use committee (protocol # 2018-0082). OVX (n = 7) and SHAM OVX (n = 7) female Sprague Dawley rats (12 weeks-old) were obtained from Charles River (Wilmington, MA). The ovariectomy procedure was performed by the vendor, Charles River, and the surgical process overseen by the Charles River Institutional Animal Care and Use Committee [19]. Animals were monitored post-operatively for one week prior to shipment. Animals were tagged and incision clips removed 2 weeks post-operatively under isoflurane anesthesia (2-3% to effect). Animals were housed communally with a density of up to 4 animals per cage. Animal Care Systems "Optirat Plus" IVC cages

were housed in a BioBubble with maintained temperature and 12-h light/dark cycle. Cages were set up in a with exhaust augmentation to ensure sufficient air turnover within each cage. Animals were given cardboard enrichment and daily human interaction. A standard rodent chow diet and water were provided ad libitum.

Sixteen weeks after ovariectomy and sham surgeries, the rats were anesthetized via isoflurane inhalation (3.5%) and euthanized via cardiac exsanguination. The right proximal tibial metaphases were scanned in vivo with microcomputed tomography (μCT) (Bruker Skyscan 1276) with a voxel size of 18 μm, x-ray tube voltage of 100 kV, current of 200 μA, 0.5 degree step size, 1 mm aluminum filter, and exposure time of 350 ms. The region of interest for trabecular bone analyses had a height of 1.6 mm starting 2 mm distal to the proximal tibial physis. Trabecular bone volume fraction, trabecular number, thickness, and spacing, and bone mineral density were quantified for each tibia. Uterii were examined and weighed to confirm ovariectomy procedure was effective [20]. SHAM OVX rats had a higher (p < 0.0001) wet uterus weight of 0.581 ± 0.082 g, while OVX rats had a visibly thinner uterus structure with a weight of 0.095 ± 0.013 g.

2.2   OVX rMSC isolation

Immediately after euthanasia, rMSCs were isolated from the bone marrow of the humerus of each rat. Briefly, the humerii from each rat was removed, the ends of the bone cut, and the bone marrow flushed with growth media and plated directly onto tissue culture plates. rMSCs were cultured in alpha modified Eagle medium (alpha-MEM, Stem Cell Technologies) with nucleosides supplemented with 50 μg/mL penicillin (Gibco), 50 μg/mL streptomycin (Gibco), and 1 μg/mL fungizone (Gibco) containing 10% (vol/vol) fetal bovine serum (Gibco). Media was changed every 2-3 days. After 10 days (70-80% confluency), rMSCs from each individual rat were frozen down in a solution of 40% growth media, 40% FBS and 20% DMSO. Passage 1 (P1) rMSCs from individual rats were pooled, expanded for an additional 7-10 days, and frozen at P2 in Cell Freezing Medium (ThermoFisher). All experiments used P3 pooled SHAM and OVX rMSCs.

2.3   Macromer synthesis

The synthesis of tetra-arm poly(ethylene glycol) (PEG)-azide and eight-arm PEG-dibenzocyclooctyne (DBCO) was performed according to previously published procedures [21-23]. Briefly, four-arm PEG amine (Mn~10,000 Da, JenKen) was dissolved in cooled dichloromethane (DCM), followed by the sequential addition of triethylamine and methanesulfonyl chloride. After O/N stirring at room temperature (RT), the reaction was diluted with DCM and washed with brine. The organic phase was dried, filtered, and concentrated under vacuum. Residual oil was precipitated into diethyl ether, centrifuged, and washed with excess ether to give mesylated PEG. ^{1}H NMR analysis was used to determine end group functionalization. Next, tetra-arm PEG-mesylate and sodium azide were dissolved in anhydrous dimethylformamide (DMF) and stirred for 48 hours at 60°C. The solution was dialyzed against deionized (DI) water (MWCO 3.5 kDa) for seven days and lyophilized. Complete disappearance of end-group mesyl protons on ^{1}H NMR was interpreted as quantitative conversion of tetra-PEG-mesylate to tetra-PEG-azide.

Eight-arm PEG amine (Mn~20,000 Da, JenKem), HATU (MilliporeSigma), and c6-DBCO-acid (Click Chem Tools) were dissolved in DMF. Methylmorpholine was added to this solution and the reaction was left overnight to stir under inert gas. Macromers were precipitated directly into diethyl ether, collected by centrifugation, dialyzed in the dark against DI water (MWCO 8 kDa), and lyophilized.

An azide modified lysine analog (Fmoc-azide-L-lysine, ChemImpex) was used to synthesize an azide-labeled RGD (N_3-KGRGDS) using standard Fmoc chemistry and a Rink Amide MBHA resin (Chempep Inc, USA) on a Protein Technologies Tribute Peptide Synthesizer. The peptides were purified using reverse phase High Pressure Liquid Chromatography (HPLC) and confirmed using negative Electrospray Ionization (ESI) mass spectroscopy.

2.4 Microgel scaffold fabrication

Microgels were synthesized as previously described[17]. Briefly, individual microgels were created using an inverse suspension polymerization with PEG-DBCO and PEG-N_3 macromers in hexanes with Span-80 (2.25% v/v) and Tween-20 (0.75% v/v). Two distinct sets of microgels, one with excess DBCO and the other with excess azide, were prepared with 11mM excess of either functional group in the polymer mix. The two populations of microgels are subsequently mixed to covalently assemble the scaffold. For DBCO excess microgels, 3mM of 8 arm 20kDa PEG-DBCO and 3mM of 4 arm 10kDa PEG-Azide were used. For azide excess formulations, 2mM of 8 arm 20kDa PEG-DBCO and 6.5mM of 4 arm 10kDa PEG-Azide. 1mM of N_3-GRGDS was included in all microgels. Shear force, either through magnetic stirring, vortexing, or sonicating respectively, was applied during polymerization to create microgels of various sizes. Microgels fabricated 40 mM Azide modified Alexaflour 647 were imaged using a Laser Scanning Confocal Microscope (Zeiss) and average microgel diameters were quantified using ImageJ software (Figure S1).

Microgels were washed (under sterile conditions) with isopropanol (4 times) and with PBS (2 times) before resuspension in PBS. Probe sonication was used before resuspension in PBS on occasion to break apart any aggregates. Microgels in PBS were used for rMSC assembly.

2.5 rMSC microgel scaffold assembly

rMSC-laden microgel scaffolds were prepared by suspending cell solutions, either 1 million OVX or SHAM rMSCs, with both microgel populations, DBCO-excess and N_3-excess microgels (~50 μL polymer mix each) swollen in PBS and centrifuging. After centrifugation, scaffolds were immediately placed in rMSC culture media (described in Section 2.2). The swollen scaffolds reached a final swollen volume of ~200μL, and a corresponding density of 5 million cells/ mL. rMSC culture media was changed 24 hours after assembly.

2.6 Osteogenic and adipogenic differentiation of OVX and SHAM rMSCs

To confirm the adipogenic bias of rMSCs isolated from OVX rats, SHAM and OVX rMSCs were differentiated into osteogenic and adipogenic lineages using a commercially available kit following the manufacturer's instructions (R&D Systems # SC020). Briefly, rMSCs were seeded on fibronectin coated glass coverslips (n=3) at a density of 4000

cells/cm^2 and cultured to ~60% and ~100% confluency for osteogenic and adipogenic differentiation conditions, respectively. Media was replaced with osteogenic and adipogenic media formulations (provided from manufacturer) every 3-4 days for up to 21 days.

2.7 RNA isolation and RT-qPCR

RNA was collected from Day 0 (24 hours after seeding) on TCPS (n=3) and 4 days after culture in microgels using the RNeasy Micro Kit (n=3) (Qiagen, Cat. No. 74004). RNA quantity and purity were determined via spectrophotometry (ND-7 1000; NanoDrop). 2 ng/uL of complementary DNA (cDNA) was synthesized using the iScript Synthesis kit (Bio-Rad, Cat. No. 1708841) on an Eppendorf Mastercycler. RT-qPCR was performed using SYBR Green reagents (Bio-Rad, Cat. No. 1708884) on an iCycler (BioRad). Relative mRNA expression levels were calculated as 2^(– Ct) from three technical replicates per condition normalized to GAPDH and each respective SHAM condition. Primer sequences are listed in Table 1.

2.8 Alkaline phosphatase (ALP) detection

ALP detection was performed on OVX and SHAM rMSCs (n=3) cultured in osteogenic conditions for 14 days using a commercially available kit (Sigma-Aldrich SCR004). Briefly, the samples were fixed in 4% paraformaldehyde (PFA) for 2 min and rinsed with Tris Buffered Saline (TBS) + 0.05% Tween 20 (TBST). A 2:1:1 mixed on Fast Violet Red (0.8g/L stock): Napthol AS-BI phosphate solution (4mg/mL) in AMPD buffer (2mol/L:water) was added to the samples for 15 min. After an additional wash with TBST, the samples were stored in PBS. Images were obtained using a 20x air objective Nikon Eclipse TE300 microscope and the % ALP area was quantified using ImageJ.

2.9 Alizarin Red

Alizarin Red staining was performed at Day 21 to detect the deposited mineralized extracellular matrix by SHAM and OVX rMSCs cultured in osteogenic inductive medium (n=3). Samples were fixed in 4% PFA for 15 min at RT and washed with PBS 3x. They were then incubated in a 40 mM solution of Alizarin Red (Sigma Aldrich TMS-008) in distilled water (pH 4.2) for 15 min. Samples were washed with PBS and images were obtained using a 20x with a Nikon Eclipse TE300 microscope. The % Alizarin red area was quantified using ImageJ.

2.10 Immunofluorescence staining

Samples were fixed for 30 min using 4% PFA or 10% formalin for rMSCs cultured on coverslips (n=3) or in microgel scaffolds (n=3), respectively. Samples were washed with PBS 3x for 10 min each. Permeabilization and blocking were performed each for 1 hour at RT in 0.1% TritonX-100 in PBS and 5% bovine serum albumin (BSA) in PBS, respectively. Mouse Anti-N-cadherin (Sigma Aldrich, 10μg/mL), Goat Anti-Mouse FABP4 (R&D systems, 10μg/mL), Rabbit anti-CD73 (Abcam, 1:100), Mouse anti-CD90 (Invitrogen, 1:250), Rabbit anti-CD45, (ThermoFisher, 1:500), and Mouse anti-CD105 (Abcam 1:100) primary antibodies in Cell Staining Buffer (Biolegend) were incubated with rocking overnight at 4°C. The next day, three washes in PBS with 0.05% Tween 20 (PBST)

for 10 min each was performed. Then, secondary antibodies (specifically, goat anti-mouse Alexaflour 488 or chicken anti-goat Alexaflour 647 (1:500), DAPI (1:500), Rhodamine Phalloidin (1:300), were incubated for 1 hour at RT. Samples were washed with PBST 3x for 5-10 min. Images were acquired using either the Operetta (Perkin Elmer) for 2D samples or a Nikon Spinning Disc Confocal (40x air objective) or a Laser Scanning Confocal Microscope (20x water objective) for 3D microgel samples.

2.11 Image Analysis

Percent Positive: For % positive analysis (%FABP4+), DAPI and Rhodamine Phalloidin staining were used to determine the nuclear and cytoplasmic areas using the Harmony software (Perkin Elmer). A single in focus plane was chosen and cell number was determined by the number of nuclei. The number of positive cells were determined by the cytoplasm stained with FABP4. Percent of FABP4 was calculated for each field of view and analyzed.

N-cadherin intensity: For rMSCs cultured on 2D TCPS, N-cadherin intensity measurements were determined using Harmony software (Perkin Elmer). Briefly, N-cadherin intensity values were measured from the cytoplasmic areas of cells in single in focus plane. For rMSCs cultured in microgels, a maximum intensity projection of approximately 80-100 μm z-stack images (with <1 μm intervals between slices) was created and N-cadherin intensity values were measured using Fiji. Outlier analysis was conducted using the ROUT method and Q=1%.

Cluster size and percentage: Cluster size and % of cells in cluster were determined using IMARIS 3D visualization software (Bitplane). Approximately 80-100 μm z-stack images (with <1 μm intervals between slices) were imported into the software and 3D surfaces around a cluster was created using the F-actin stain. Next, the nuclei were marked using DAPI staining and the Spot Analysis feature of IMARIS. Using a pre-written Matlab code (Split into Surface Objects Xtension) within the IMARIS software, the number of nuclei within each cluster (defined as >3 nuclei) was determined.

2.12 Secretory Analysis

Global secretory profiles were measured using a Rat Cytokine Array C2 (RayBiotech) and the manufacturer's protocol was followed. Briefly, arrays were blocked for 30 min at RT and incubated overnight at 4°C with 1 mL of conditioned media (pooled from n=3 microgel scaffolds) collected after three days of rMSC culture in microgel scaffolds. The next day, the membranes were washed, incubated with a biotinylated antibody cocktail for 1.5 hrs at RT, washed, and then incubated with HRP-streptavidin for 2 hrs at RT. Chemiluminescence signal from the membranes was detected using a charge-coupled device camera (ImageQuant LAS 4000 GE Healthcare).

Analysis was performed using the manufacture's guidance. Spot intensity values from raw images were determined using the 2D Array feature of ImageQuant (GE Healthcare). The relative intensities were calculated as using the manufacturer's recommended method (Raybiotech). For each array, the background signal from negative control spots was

subtracted and average intensities were normalized to positive spot controls on each array. Next, the intensity values for each sample array were normalized control (blank media) arrays. Finally, raw normalized intensity values were compared between OVX and SHAM samples, either by plotting in a heatmap or calculating the log fold change between samples. ELISAs were performed according to the manufacturer's protocol for TIMP-1 and MCP-1 (R&D systems, Rat Duo ELISA kits).

2.13 N-cadherin blocking

Blocking of N-cadherin cell-cell interactions were performed using an anti-N-cadherin antibody following previously published protocols[18,23]. Briefly, rMSCs were trypsinized, re-suspended in growth media containing N-cadherin blocking antibody (50 μg ml^{-1}, Sigma-Aldrich GC4), and incubated for 45 min at 4°C. The cells were then washed twice with PBS and assembled with microgels networks or plated on glass coverslips. It is important to note that 10 μg/mL of the N-cadherin blocking antibody was also included in the media throughout the experiments to ensure sustained blocking.

2.14 Protein isolation and western blot

Protein was collected from Day 0 (24 hours after seeding) on TCPS (n=3) and 4 days after culture in microgels (n=3) using the cold RIPA Buffer (Thermo Fisher Scientific) supplemented with Halt protease, phosphatase inhibitor (Thermo Fisher Scientific). Cells were lysed for 20 min, the lysate was collected, vortexed for ~30sec, and incubated on ice for an addition 15 min. Lysate was centrifuged at 20,000xg for 10 min, supernatant was moved toa new tube, flash frozen and stored at −20°C until use. Protein concentration was quantified using a Pierce Micro BCA Protein kit (Thermo Fisher Scientific) according to manufacturer's instructions and the plate was imaged at 562 nm using a Synergy F1 hybrid reader (BioTek).

10 μg of protein was denatured in 1x Laemmli SDS sample buffer (Alfa Aesar) supplemented with 1mM dithiothreitol (DTT, Bio-Rad) boiled for 5 min at 96 °C. Proteins were separated using polyacrylamide Precast Protein Gels (Bio-Rad) in SDS running buffer consisting of 25 mM Tris-Base (Fisher Scientific), 192mM glycine (Bio-Rad), 0.1% sodium dodecyl sulphate (Fisher Scientific) under 130 V for 60 min. Proteins were transferred to a pre-cut PVDF membrane (BioRad) in cold transfer buffer consisting of 25 mM Tris (Fisher Scientific), 192 mM glycine (Bio-Rad), 10% methanol for 60 minutes at 80V. Membranes were blocked in a 5% skim milk powder in TBS at room temperature for 1 hour at RT. Primary antibodies, specifically, Mouse anti- GAPDH (Abcam, 1:1000 dilution) and Rabbit Anti-N-cadherin (Abcam, 1 μg/mL), in 5% skim milk powder in TBS at 4 °C overnight on a shaker. The next day, the membranes was washed in TBST (0.1% TWEEN-20 in TBS buffer) and incubated with secondary goat-anti- mouse or rabbit HRP conjugated antibody (at a concentration 3 times more diluted than the primary antibody) for 1 hour at room temperature depending on the host of the primary antibody. Chemiluminescence signal was detected using Pierce ECL Plus solution (ThermoFisher Scientific) and an ImageQuant LAS 4000 detector. The band signal was quantified using the Gels Plug in on the ImageJ software.

2.15 Statistical Analysis

Statistical analysis and data visualization was done using Graphpad v9. A two-way ANOVA with multiple comparisons were used to determine statistical significance between SHAM and OVX (Factor 1) and microgel conditions (Factor 2) for cell cluster size and %cells in a cluster (Figure 1). One-way ANOVAs with Tukey ad hoc tests were performed to determine statistical significance for secretion and gene expression data. N=3 technical replicates are plotted with standard mean error unless otherwise noted.

3 RESULTS

3.1 Ovariectomy induced trabecular bone loss

Sixteen weeks after Sprague-Dawley rats underwent an ovariectomy (OVX) or sham (SHAM) surgeries, microcomputed tomography was performed on the trabecular regions (starting 2 mm distal to the proximal tibial physis) for each of the rats (Figure S1a). μCT images were reconstructed using NRecon, saved in DataViewer, and analyzed using CTan. Rats that underwent the OVX surgery (OVX rats) had significantly lower bone mineral density (Figure S1b) and bone volume (Figure S1c) compared to rats that underwent a sham surgery (SHAM rats). Properties of the trabeculae were also altered. The number of trabeculae per unit length, or trabecular number, was significantly decreased in (Figure S1d) and the spacing between individual trabecula was increased in OVX rats (Figure S1e). Interestingly, no differences in trabecular thickness was observed, as both SHAM and OVX rats had 0.09 mm thick trabeculae.

3.2 OVX rMSCs are biased towards adipogenic fates

rMSCs were isolated from the bone marrow of the humerii of OVX and SHAM rats immediately after euthanasia. Cells isolated from both OVX and SHAM rats were positive for classic MSC markers (CD90, CD105, and CD73) and were negative for CD45, a hematopoietic stem cell marker (Figure S2). After 14 days in osteogenic media, gene expression of *Runx2*, a key osteogenic transcription factor, was significantly lower in OVX rMSCs (Figure S3a) compared to SHAM. In adipogenic media, expression of *Pparg* and *Fabp4*, both markers of adipocyte differentiation, were significantly higher in OVX rMSCs compared to SHAM. Protein expression of FABP4 was also significantly increased in OVX rMSCs at Day 14 relative to SHAM (Figure S3b). A marker of osteogenic differentiation, ALP activity, was significantly decreased in OVX rMSCs in osteogenic media conditions at Day 14 (Figure S3c). Lastly, calcified matrix deposition, as measured by Alizarin Red at Day 21 was also significantly decreased in OXV rMSCs relative to SHAM. Collectively, these results confirmed the increased adipogenic potential and decreased osteogenic potential of OVX rMSCs compared to SHAM controls.

3.3 Granular porous scaffolds with varied particle sizes direct rMSC clustering

After OVX and SHAM rMSCs were cultured on TCPS for four days, 97% of the secreted cytokine and growth factors measured as low or undetectable concentrations (Figure S4); necessitating an alternative culture platform to study their secreted factors. Prior literature has suggested that MSCs cultured in three-dimensional biomaterial scaffolds, with a network

on interconnected pores, can better maintain and even increase MSC secretory properties by promoting cell-cell interactions [10,17].

For this reason, we utilized a cell-adhesive microgel scaffold with varying pore sizes to cluster and culture OVX and SHAM rMSCs in 3D. The porous scaffolds were assembled from microgels by using a SPAAC reaction between multi-arm PEG macromers end functionalized DBCO or azide under varying degrees of shear (Figure 1a). Specifically, stirring resulted in large microgel diameters of 210 μm ± 109 μm (~200 μm), vortexing resulted in medium microgel diameters of 102 μm ± 43 μm (~100 μm), and sonicating resulted in microgel diameters of 14 μm ± 9 μm (~10 μm) (Figure S5). Previous work thoroughly characterizing these materials and the various fabrication methods do not show any changes to surface roughness[17]. Upon assembly with rMSCs (~5million cells/mL), the cells become embedded in the void spaces (or pores) and interact with the RGD motifs (1 mM) on the microgels (Figure 1b). After four days, rMSCs cultured in scaffolds comprised of microgels with average diameters of ~10 μm reside largely as single cells (Figure 1c, left). rMSCs in scaffolds comprised of microgels with increasing average diameters, ~100 μm and ~200 μm, form progressively larger clusters (Figures 1c, middle, right).

Using a 3D rendering software, IMARIS, the degree of cell clustering (Figure 1d) and cluster size (Figure 1e) were quantified for both SHAM and OVX rMSCS. Here, we defined a cluster as three or more nuclei (blue) contained within the same F-actin region (red). Less than 25% of SHAM and OVX rMSCs in 10 μm scaffolds resided in a cluster (~3 cells), indicating rMSCs reside as mostly single cells in these scaffolds. In 100 μm scaffolds, 47.8% ± 17.1% of SHAM rMSCs and 36.0% ± 2.7% of OVX rMSCs resided in clusters, and these clusters contain ~5 cells. In scaffolds prepared with the 200 μm microgels, the OVX rMSCs had nonsignificantly higher degree of clustering (95.0% ± 2.1% with ~30 ± 10 cells) relative to SHAM cells (84.1% ± 7.3%, ~20 ± 7 cells). A two-way ANOVA analysis revealed that both the degree of clustering and the cluster size were significantly varied between the three microgel conditions. However, there were no statistical differences (p> 0.05) between the clustering phenotypes of SHAM and OVX rMSCs in each microgel condition, suggesting that any observed secretory differences are not due to differences in the extent of clustering. For the remainder of the discussion, the conditions will be referred to as large clusters for rMSCs assembled with the 200 μm microgel diameter scaffolds, small clusters for rMSCs assembled with the 100 μm microgel scaffolds, and single cells for rMSCs assembled with the 10 μm microgel scaffolds.

3.4 Clustering increases global cytokine secretion in both OVX and SHAM rMSCs, but the increases are more pronounced in OVX rMSCs

After establishing three clustering phenotypes by varying the microgel pore dimensions, we next explored how clustering phenotypes impacted OVX and SHAM rMSC secretory properties. We measured the secretory properties of SHAM and OVX rMSCs cultured as large clusters (~30 cells/cluster), as small clusters (~5 cells/cluster), and as single cells using a cytokine array (RayBiotech Rat C2, Figure S6). Both SHAM and OVX rMSCs in large clusters had elevated secretion of a majority of the measured secreted factors (Figure 2a). For SHAM rMSC conditions, out of the 34 secreted factors measured, 79% were most

elevated in the large clusters, followed by ~15% in the small clusters and ~6% in the single cells (Figure 2b, top). For the OVX rMSCs conditions, 97% of the measured factors were most elevated in large clusters, only ~3% in small clusters, and zero in the single cells (Figure 2b, bottom). These results indicate that in large clusters, OVX rMSC secretory properties are more pronounced than those of the SHAM controls. Next, we sought to analyze the differences between the SHAM and OVX rMSC secretory profiles in greater detail.

3.5 OVX rMSCs have elevated secretion of pro-resorptive cytokines in large clusters relative to SHAM

To further explore whether an altered secretory profile from OVX rMSCs may be involved in their pro-resorptive bias, we identified a subset of factors that have pro-resorptive functions (Figure 3a). Many of the pro-resorptive factors are secreted by both SHAM and OVX cells cultured as single cells or in small clusters had a similar profile. However, in the large clusters, larger differences are observed between the SHAM and OVX rMSCs (Figure 3b, pro-resorptive factors labelled in red).

Notably, 6 of the 10 pro-resorptive factors, Activin A, CXCL1, CX3CL1, MCP-1, TIMP-1, and TNF-alpha, are greatly elevated in OVX rMSC clusters relative to SHAM (Figure 3b). There were no differences in the secretion of IL-1, IL-1a, IL-1b, and IL-6, indicating that pro-inflammatory interleukin secretion may not be significantly altered in OVX rMSCs. Additionally, secretion of VEGF-A, an angiogenic factor present in bone marrow adipose tissue, was elevated in the OVX rMSCs compared to SHAM rMSCs. Four of the top five most elevated factors in large clusters of OVX compared to SHAM rMSCs are classified as pro-resorptive and are not greatly altered when OVX and SHAM rMSCs are cultured as single cells or in small clusters (Figure 3c). Collectively, these results indicate that the secretory profile of OVX rMSCs is biased towards a pro-resorptive phenotype. However, we note that the differences in the secretory profile are not present when OVX and SHAM rMSCs are cultured in small clusters or as single cells (Figure S7), indicating that cell-cell contacts may be involved in the production of pro-resorptive cytokines by OVX rMSCs.

3.6 N-cadherin expression is significantly elevated in OVX rMSCs compared to SHAM rMSCs

After culturing SHAM and OVX rMSCs on TCPS for 4 days in growth conditions, RT-qPCR was performed for a variety of cadherin genes (Figure 4a). In general, both SHAM and OVX expressed *Cdh1* (E-cadherin), *Cdh2* (N-cadherin), *Cdh5* (VE-cadherin) *Cdh11* (OB-cadherin), *Cdh13* (T-cadherin), and *Cdh15* (M-cadherin) and, notably, did not express *Cdh4*. Only *Cdh2*, or N-cadherin, gene expression was ~4 fold higher in OVX rMSCs relative to SHAM, which was further observed at the protein level by immunostaining (Figure 4b). Image quantification confirmed an overall higher fluorescence intensity of N-cadherin by OVX rMSCs relative to SHAM (Figure 4c). Based on these results, we investigated N-cadherin expression in the 3D porous microgel scaffolds as a function of rMSC clustering.

3.7 N-cadherin expression is elevated in clustered and single OVX rMSCs relative to SHAM rMSCs

We next measured N-cadherin expression in the 3D porous microgel scaffolds, where rMSCs were cultured either as single cells or as large clusters for both OVX and SHAM rMSCs. Representative images show increased N-cadherin expression for single OVX rMSCs cultured in the 10 μm microgel scaffolds compared to SHAM single cells (Figure 4d, left). This quantification of this observation can be found in Figure 4e. *Cdh2* gene expression was also ~4 fold higher in single OVX rMSCs relative to single SHAM cells (Figure 4f). These trends were also observed in the large rMSC clusters in ~200 μm microgel scaffolds (Figure 4 d,e,f) and for small rMSC clusters in ~100 μm microgels scaffolds (Figure S8). Further, western blot analysis was also conducted to confirm the elevated N-cadherin in OVX rMSCs (Figure S9). Overall, we observed that OVX rMSCs maintained their elevated N-cadherin expression relative to SHAM cells, both when cultured as single cells, small clusters, and large clusters of cells.

3.8 Blocking N-cadherin reduces secretion of pro-resorptive cytokines in OVX rMSCs clusters

As N-cadherin expression is higher in OVX rMSCs, both as single cells and as large clusters, we next sought to determine the specific role of N-cadherin on MSC secretory properties and profiles. To do this, we blocked N-cadherin before assembling OVX and SHAM rMSCs with 200 μm microgel scaffolds, where they reside as large cell clusters. After 4 days of culture, cytokine and growth factor secretion was measured. Results showed a significant decrease in overall secretion in OVX rMSCs relative to SHAM cells (Figure 5a). In contrast to the secretory profiles seen before (Figure 3b), when N-cadherin interactions were blocked, large clusters of OVX rMSCs no longer produced higher levels of pro-resorptive cytokines relative to SHAM cells in the same conditions. This reduction was not observed when N-cadherin was blocked in OVX rMSC cultures as single cells (Figure S10). Approximately no change or a decrease in secretion was observed for the previously five most elevated factors by OVX rMSCs in large clusters (Activin A, CXCL1, MCP1, TIMP1 and VEGF-A) when N-cadherin was blocked (Figure 5b).

To test whether the global decreases were due to a lack of secretion from both cell types, increases by SHAM rMSCs, or a decrease by OVX rMSCS only, we performed ELISAs to quantify the concentrations of TIMP-1 (Figure 5c) and MCP-1 (Figure 5d). For both factors, blocking N-cadherin resulted in selective decreased secretion by OVX rMSCs in large clusters, while SHAM rMSCs maintained their secretory levels compared to their respective unblocked controls. Overall, these results indicate that N-cadherin interactions are necessary for the pro-resorptive bias of the secretory profile of OVX rMSCs.

4 DISCUSSION

Patients with postmenopausal osteoporosis have higher bone resorption rates and higher fracture risk, potentially due to impairments in their MSC functional properties [2]. As factors secreted by MSCs are known to be involved in bone healing and homeostasis, we characterized the secretory profile of OVX rMSCs utilizing porous granular hydrogels to

cluster rMSCs (single cells to ~30 cells/cluster) with varying percentages of cells within clusters (~20-90%) (Figure 1). OVX rMSCs cultured in scaffolds with pore dimensions designed to increase cell clustering secreted higher concentrations of several factors relative to single cells (Figure 2), specifically pro-resorptive and anti-osteogenic factors (Figure 3). As the pro-resorptive bias of the OVX rMSC secretory profile was only observed in large cell clusters, we further sought to understand if cadherin mediated cell-cell connections were involved. N-cadherin was highly expressed in OVX rMSCs compared to SHAM cells (Figure 4). Furthermore, blocking N-cadherin suppressed the pro-resorptive bias of the OVX rMSC secretory profile (Figure 5).

While the *in vivo* identity of MSCs is not fully understood, it is of high likelihood that MSCs in contact with bone participate in N-cadherin signaling with other cell types in the bone marrow niche[9,18]. To maintain bone homeostasis, MSCs interact with bone lining cells and osteoblasts—which have high N-cadherin expression[9,24]—and can secrete factors to direct activities of nearby cells, including immune cells, osteoblasts, osteoclasts, and other MSCs. As we are interested in exploring this secretory signaling *in vitro*, we chose to cluster MSCs in granular hydrogels to control their N-cadherin binding. In this study, we observed that OVX rMSCs in large clusters (partially mediated through N-cadherin interactions) secrete TNF-α, TIMP-1, and CXCL1, factors known to inhibit osteoprogenitor proliferation, differentiation, and mineralization [25-27]. OVX rMSCs also secreted elevated levels of several factors that can promote osteoclast fusion, such as Activin A and MCP-1, increasing rates of bone resorption [28,29]. Additionally, TNF-α, CXCL1, MCP-1, and CX3CL1 can direct macrophage and lymphocyte migration and pro-inflammatory polarization[30,31], which can increase inflammation and lead to higher bone resorption rates. However, it is important to note that not all elevated factors were dependent on N-cadherin signaling. For example, we observed elevated levels of Fas Ligand, an initiator of T-cell apoptosis, in OVX rMSCs relative to SHAM cultured both on TCPS (Figure S4) and as single cells with blocked N-cadherin interactions (Figure S10).

Interestingly, typical levels of many of the factors measured in this study are also known to be disrupted globally in osteoporotic patients. Serum analysis revealed increased TNF-α in osteoporotic women compared to age matched controls [32]. Additionally, VEGF-A, MCP-1, and TNF- α levels were elevated in white adipose tissue isolated from OVX rats [33]. MCP-1 expression is also elevated in immune cells in bone marrow fat, which can contribute to an inflammatory environment [34]. While it is improbably that MSCs are solely responsible for these elevations—as they are present in very few numbers *in vivo*— MSCs likely have significant local effects in the bone marrow niche, including both direct effects, such as osteoblast and adipocyte differentiation, and indirect secretory effects, such as osteoprogenitor proliferation and osteoclast fusion. However, their role in the pathogenesis of osteoporosis requires further elucidation.

One potential implication from this study goes beyond the investigation of the OVX rMSC secretory profile; namely, that the binding of N-cadherin may be necessary for MSC secretome elevation. Even though OVX rMSCs cultured across multiple platforms expressed elevated levels of N-cadherin relative to their SHAM counterparts (Figures 4), their secretory properties were only elevated when cultured as large clusters (Figure

2). Additionally, blocking N-cadherin interactions resulted in reduced secretion from OVX rMSCs solely in large clusters (Figure 5) and not in single cells (Figure S10). Molecularly, the homotypic binding of N-cadherin initiates the formation of the cadherin catenin complex, resulting in the sequestration of α- and β-catenin in a force-dependent manner [35]. α-catenin can bind to F-actin, thus linking the cadherin-catenin complex to the cytoskeleton, where applied tension can result in downstream gene expression [36]. Additionally, β-catenin can interact with multiple transcriptional pathways, including Wnt [37-39] and NF-κB [25,40], which both regulate transcription of numerous secreted factors. Taken together, these results indicate that overexpression of N-cadherin may not be enough to elevate MSC secretion, but rather N-cadherin binding, facilitated through cell clustering, must occur. Therefore, MSC clustering may be an important strategy for cell-based therapeutics relying on their secreted factors and aid in the improvement of biomaterial delivery systems.

5 CONCLUSIONS

Secreted factors from bone marrow resident MSCs can influence bone homeostasis, including rates of bone resorption and deposition, which are altered in osteoporosis. Here, we utilized porous granular hydrogel scaffolds to control both the degree of cell clustering (~20-90%) and the size of clusters (single cells-30 cells/cluster). We observed increased secretion of Activin A, CXCL1, CX3CL1, MCP-1, TIMP-1, and TNF-α by OVX rMSCs in large clusters compared to SHAM rMSCs, indicating a pro-resorptive bias of the OVX rMSC secretory profile. Further, we observed a four-fold elevation in N-cadherin expression in OVX rMSCs compared to SHAM, both when cultured as single cells and as large clusters. Finally, we demonstrated that N-cadherin signaling was partially responsible for the regulation of OVX rMSC secretory properties, as only large cell clusters of OVX rMSCs selectively decreased secretion of TIMP-1 and MCP-1 when N-cadherin interactions were blocked. The design of modular platforms that allow for the controlled examination of the effects of numerous parameters (i.e., cell clustering and N-cadherin interactions) on the secretory properties OVX rMSCs will significantly aid in the design of future MSC therapies for healing in osteoporotic environments.

Supplementary Material

Refer to Web version on PubMed Central for supplementary material.

Funding Sources

7 REFERENCES

[1]. Yu B, Wang CY, Osteoporosis: The Result of an 'Aged' Bone Microenvironment, Trends in Molecular Medicine. 22 (2016) 641–644. 10.1016/j.molmed.2016.06.002. [PubMed: 27354328]

[2]. Eastell R, O TW, Hofbauer LC, Langdahl B, Reid IR, Gold DT, Cummings SR, Postmenopausal osteoporosis, Nature Review Primer. (2016). 10.1038/nrdp.2016.69.

[3]. Wu D, Cline-Smith A, Shashkova E, Aurora R, Osteoporosis: A Multifactorial Disease, n.d. www.intechopen.com.

[4]. Whitfield JF, How to grow bone to treat osteoporosis and mend fractures., Curr Osteoporos Rep. 1 (2003) 32–40. 10.1007/s11914-003-0006-7. [PubMed: 16036063]

[5]. Cheung WH, Miclau T, Chow SK-H, Yang FF, Alt V, Fracture healing in osteoporotic bone, Injury. 47 (2016) S21–S26. 10.1016/S0020-1383(16)47004-X.

[6]. Park D, Spencer JA, Koh BI, Kobayashi T, Fujisaki J, Clemens TL, Lin CP, Kronenberg HM, Scadden DT, Endogenous bone marrow MSCs are dynamic, fate-restricted participants in bone maintenance and regeneration, Cell Stem Cell. 10 (2012) 259–272. 10.1016/j.stem.2012.02.003. [PubMed: 22385654]

[7]. Tewari D, Khan MP, Sagar N, China SP, Singh AK, Kheruka SC, Barai S, Tewari MC, Nagar GK, Vishwakarma AL, Ogechukwu OE, Bellare JR, Gambhir S, Chattopadhyay N, Ovariectomized Rats with Established Osteopenia have Diminished Mesenchymal Stem Cells in the Bone Marrow and Impaired Homing, Osteoinduction and Bone Regeneration at the Fracture Site, Stem Cell Reviews and Reports. 11 (2015) 309–321. 10.1007/s12015-014-9573-5. [PubMed: 25433862]

[8]. Corrigan MA, Coyle S, Eichholz KF, Riffault M, Lenehan B, Hoey DA, Aged Osteoporotic Bone Marrow Stromal Cells Demonstrate Defective Recruitment, Mechanosensitivity, and Matrix Deposition, Cells Tissues Organs. 207 (2019) 83–96. 10.1159/000503444. [PubMed: 31655814]

[9]. Cao X, Frenette PS, Mao JJ, Robey PG, Simmons PJ, Wang C-Y, Bianco P, The meaning, the sense and the significance: translating the science of mesenchymal stem cells into medicine, Nature Medicine. (2013). 10.1038/nm.3028.

[10]. Qazi TH, Mooney DJ, Duda GN, Geissler S, Biomaterials that promote cell-cell interactions enhance the paracrine function of MSCs, (2017). 10.1016/j.biomaterials.2017.06.019.

[11]. Ogle ME, Doron G, Levy MJ, Temenoff JS, Hydrogel Culture Surface Stiffness Modulates Mesenchymal Stromal Cell Secretome and Alters Senescence, Tissue Engineering Part A. (2020) ten.tea.2020.0030. 10.1089/ten.tea.2020.0030.

[12]. Rao VV, Vu MK, Ma H, Killaars AR, Anseth KS, Rescuing mesenchymal stem cell regenerative properties on hydrogel substrates post serial expansion, Bioengineering & Translational Medicine. (2018) 1–10. 10.1002/btm2.10104.

[13]. Wan Wong S, Lenzini S, Cooper MH, Mooney DJ, Shin J-W, Soft extracellular matrix enhances inflammatory activation of mesenchymal stromal cells to induce monocyte production and trafficking, 2020. http://advances.sciencemag.org/ (accessed June 28, 2020).

[14]. Qazi TH, Mooney DJ, Duda GN, Geissler S, Biomaterials that promote cell-cell interactions enhance the paracrine function of MSCs, Biomaterials. 140 (2017) 103–114. 10.1016/j.biomaterials.2017.06.019. [PubMed: 28644976]

[15]. Gionet-Gonzales MA, Leach JK, Engineering principles for guiding spheroid function in the regeneration of bone, cartilage, and skin, Biomedical Materials (Bristol). 13 (2018). 10.1088/1748-605X/aab0b3.

[16]. Ho SS, Murphy KC, Binder BYK, Vissers CB, Leach JK, Increased Survival and Function of Mesenchymal Stem Cell Spheroids Entrapped in Instructive Alginate Hydrogels, Stem Cells Translational Medicine. 5 (2016) 773–781. [PubMed: 27057004]

[17]. Caldwell AS, Rao V. v., Golden AC, Anseth KS, Porous bio-click microgel scaffolds control hMSC interactions and promote their secretory properties, Biomaterials. 232 (2020) 119725. 10.1016/j.biomaterials.2019.119725. [PubMed: 31918222]

[18]. Qazi TH, Mooney DJ, Duda GN, Geissler S, Niche-mimicking interactions in peptide-functionalized 3D hydrogels amplify mesenchymal stromal cell paracrine effects, Biomaterials. 230 (2020). 10.1016/j.biomaterials.2019.119639.

[19]. Charles River, Ovariectomy, Surgery Code: OVARIEX, (2017). https://www.criver.com/sites/default/files/resource-files/ovariectomy.pdf.

[20]. Lemini C, Jaimez R, Figueroa A, Martinez-Mota L, Avila ME, Medina M, Ovariectomy differential influence on some hemostatic markers of mice and rats, Exp Anim. 64 (2015) 81–89. 10.1538/expanim.14-0052. [PubMed: 25312504]

[21]. Rossow T, Seiffert S, Supramolecular polymer gels with potential model-network structure, Polymer Chemistry. 5 (2014) 3018–3029. 10.1039/C3PY01692G.

[22]. Tang S, Ma H, Tu H-C, Wang H-R, Lin P-C, Anseth KS, Adaptable Fast Relaxing Boronate-Based Hydrogels for Probing Cell–Matrix Interactions, Advanced Science. 5 (2018) 1800638. 10.1002/ADVS.201800638. [PubMed: 30250802]

[23]. Caldwell AS, Campbell GT, Shekiro KMT, Anseth KS, Clickable Microgel Scaffolds as Platforms for 3D Cell Encapsulation, Advanced Healthcare Materials. 6 (2017) 1–8. 10.1002/adhm.201700254.

[24]. Pittenger MF, Discher DE, Péault BM, Phinney DG, Hare JM, Caplan AI, Mesenchymal stem cell perspective: cell biology to clinical progress, Npj Regenerative Medicine. 4 (2019). 10.1038/s41536-019-0083-6.

[25]. Chang J, Liu F, Lee M, Wu B, Ting K, Zara JN, Soo C, al Hezaimi K, Zou W, Chen X, Mooney DJ, Wang CY, NF-κB inhibits osteogenic differentiation of mesenchymal stem cells by promoting β-catenin degradation, Proc Natl Acad Sci U S A. (2013). 10.1073/pnas.1300532110.

[26]. Liang T, Gao W, Zhu L, Ren J, Yao H, Wang K, Shi D, TIMP-1 inhibits proliferation and osteogenic differentiation of hBMSCs through Wnt/β-catenin signaling, Bioscience Reports. 39 (2019) 20181290. 10.1042/BSR20181290.

[27]. Du D, Zhou Z, Zhu L, Hu X, Lu J, Shi C, Chen F, Chen A, TNF-α suppresses osteogenic differentiation of MSCs by accelerating P2Y2 receptor in estrogen-deficiency induced osteoporosis, Bone. 117 (2018) 161–170. 10.1016/j.bone.2018.09.012. [PubMed: 30236554]

[28]. Kajita T, Ariyoshi W, Okinaga T, Mitsugi S, Tominaga K, Nishihara T, Mechanisms involved in enhancement of osteoclast formation by activin-A, Journal of Cellular Biochemistry. 119 (2018) 6974–6985. 10.1002/jcb.26906. [PubMed: 29737562]

[29]. Ikenoue T, Jingushi S, Urabe K, Okazaki K, Iwamoto Y, Inhibitory Effects of Activin-A on Osteoblast Differentiation During Cultures of Fetal Rat Calvarial Cells, 1999.

[30]. Zha L, He L, Liang Y, Qin H, Yu B, Chang L, Xue L, TNF-α contributes to postmenopausal osteoporosis by synergistically promoting RANKL-induced osteoclast formation, Biomedicine and Pharmacotherapy. 102 (2018) 369–374. 10.1016/j.biopha.2018.03.080. [PubMed: 29571022]

[31]. Mosser DM, Edwards JP, Exploring the full spectrum of macrophage activation, Nature Reviews Immunology. 8 (2008) 958–969. 10.1038/nri2448.

[32]. Pino AM, Ríos S, Astudillo P, Fernández M, Figueroa P, Seitz G, Rodríguez JP, Concentration of adipogenic and proinflammatory cytokines in the bone marrow supernatant fluid of osteoporotic women, Journal of Bone and Mineral Research. 25 (2010) 492–498. 10.1359/jbmr.090802. [PubMed: 19653807]

[33]. Shen HH, Yang CY, Kung CW, Chen SY, Wu HM, Cheng PY, Lam KK, Lee YM, Raloxifene inhibits adipose tissue inflammation and adipogenesis through Wnt regulation in ovariectomized rats and 3 T3-L1 cells, Journal of Biomedical Science. 26 (2019) 1–12. 10.1186/s12929-019-0556-3. [PubMed: 30602371]

[34]. Kim W-K, Choi E-K, Sul O-J, Park Y-K, Kim E-S, Yu R, Suh J-H, Choi H-S, Monocyte Chemoattractant Protein-1 Deficiency Attenuates Oxidative Stress and Protects against Ovariectomy-Induced Chronic Inflammation in Mice, PLoS ONE. 8 (2013) e72108. 10.1371/journal.pone.0072108. [PubMed: 23977220]

[35]. Barcelona-Estaje E, Dalby MJ, Cantini M, Salmeron-Sanchez M, You Talking to Me? Cadherin and Integrin Crosstalk in Biomaterial Design, Advanced Healthcare Materials. 10 (2021). 10.1002/adhm.202002048.

[36]. Killaars AR, Walker CJ, Anseth KS, Nuclear mechanosensing controls MSC osteogenic potential through HDAC epigenetic remodeling, (n.d.). 10.1073/pnas.2006765117/-/DCSupplemental.

[37]. Hendriks D, Macdougald O, Bernkopf D, de Winter TJJ, Nusse R, Running Against the Wnt: How Wnt/β-Catenin Suppresses Adipogenesis, Frontiers in Cell and Developmental Biology | Www.Frontiersin.Org. 9 (2021) 627429. 10.3389/fcell.2021.627429. [PubMed: 33634128]

[38]. Nelson WJ, Nusse R, Convergence of Wnt,-Catenin, and Cadherin Pathways, n.d. http://science.sciencemag.org/ (accessed May 23, 2019).

[39]. Haÿ EH, Laplantine E, Geoffroy V, Frain M, Kohler T, Müller R, Marie PJ, N-Cadherin Interacts with Axin and LRP5 To Negatively Regulate Wnt/-Catenin Signaling, Osteoblast Function, and Bone Formation, MOLECULAR AND CELLULAR BIOLOGY. 29 (2009) 953–964. 10.1128/MCB.00349-08. [PubMed: 19075000]

[40]. Manuel Baizabal-Aguirre V, Tyagi AK, Hottiger MO, Ma B, Crosstalk between wnt/β-Catenin and NF-κB Signaling Pathway during inflammation, 7 (2016) 1. 10.3389/fimmu.2016.00378.
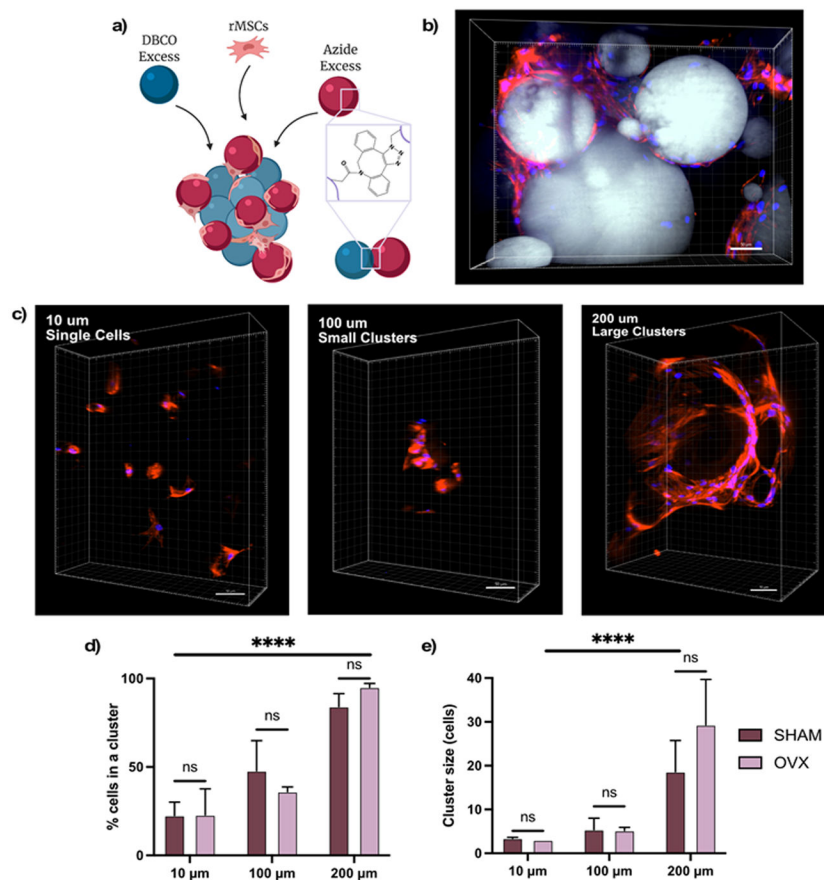
Figure 1. Porous microgel scaffolds direct rMSC clustering.
(A) Schematic of cell-laden microgel scaffolds synthesized by combing DBCO excess microgels, azide excess microgels, and rMSCs. Individual microgels and the scaffold are covalently bound with SPAAC chemistry (B) Representative image of rMSCs in 200 μm scaffolds. (C) Representative images of rMSCs cultured in 10 μm (left), 100 μm (middle), and 200 μm (right) average diameter microgel scaffolds. Quantification of (D) % cells in clusters and (E) cluster size of SHAM (black) and OVX (grey) rMSCs. Error bars represent SEM. Scale bar = 50 μm. Microgels labeled in grey, nuclei in blue, and F-actin in red. Stars represent significance across conditions using a two-way ANOVA (**** p-value <0.0001, ns – not significant)
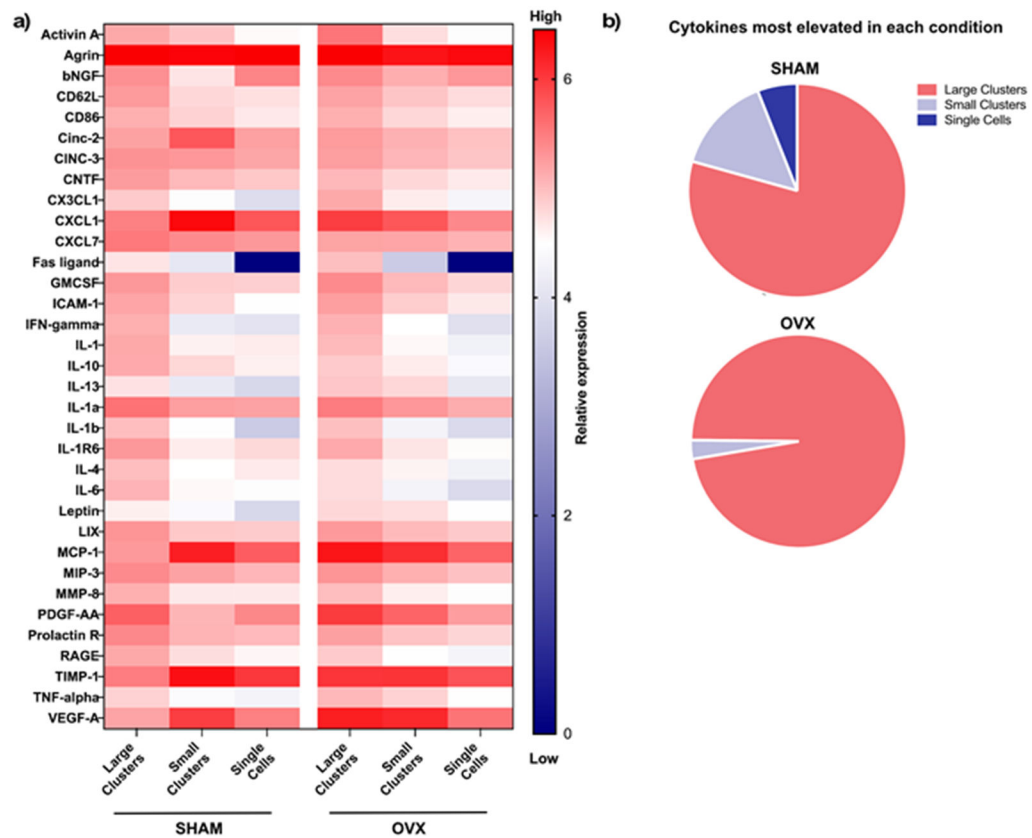
Figure 2. OVX and SHAM rMSCs secretory properties are increased in large clusters.
(A) Heatmap of concentration of cytokine array OVX and SHAM rMSCs cultured in large clusters, small clusters, and as single cells. Red represents high expression and blue represents low expression or no detection. (B) Distribution of factors most elevated in each clustering condition for SHAM (top) and OVX (bottom).
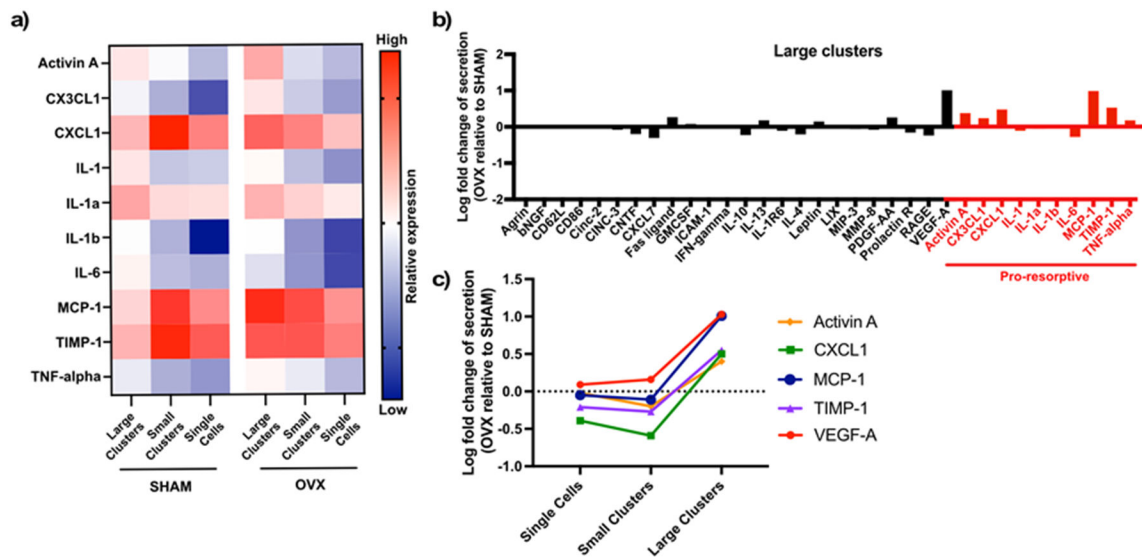
Figure 3. OVX rMSC secretory profile exhibit a pro-resorptive bias.
(A) Heatmap of pro-resorptive factor secretion from OVX and SHAM rMSC cultured as large clusters, small clusters, or single cells. (B) Log fold change of secretion of OVX rMSC in large clusters relative to SHAM rMSCs in large clusters. Factors listed in red are classified as pro-resorptive. (C) Log fold change of the top five factors most elevated by OVX rMSCs in large clusters across all clustering conditions.
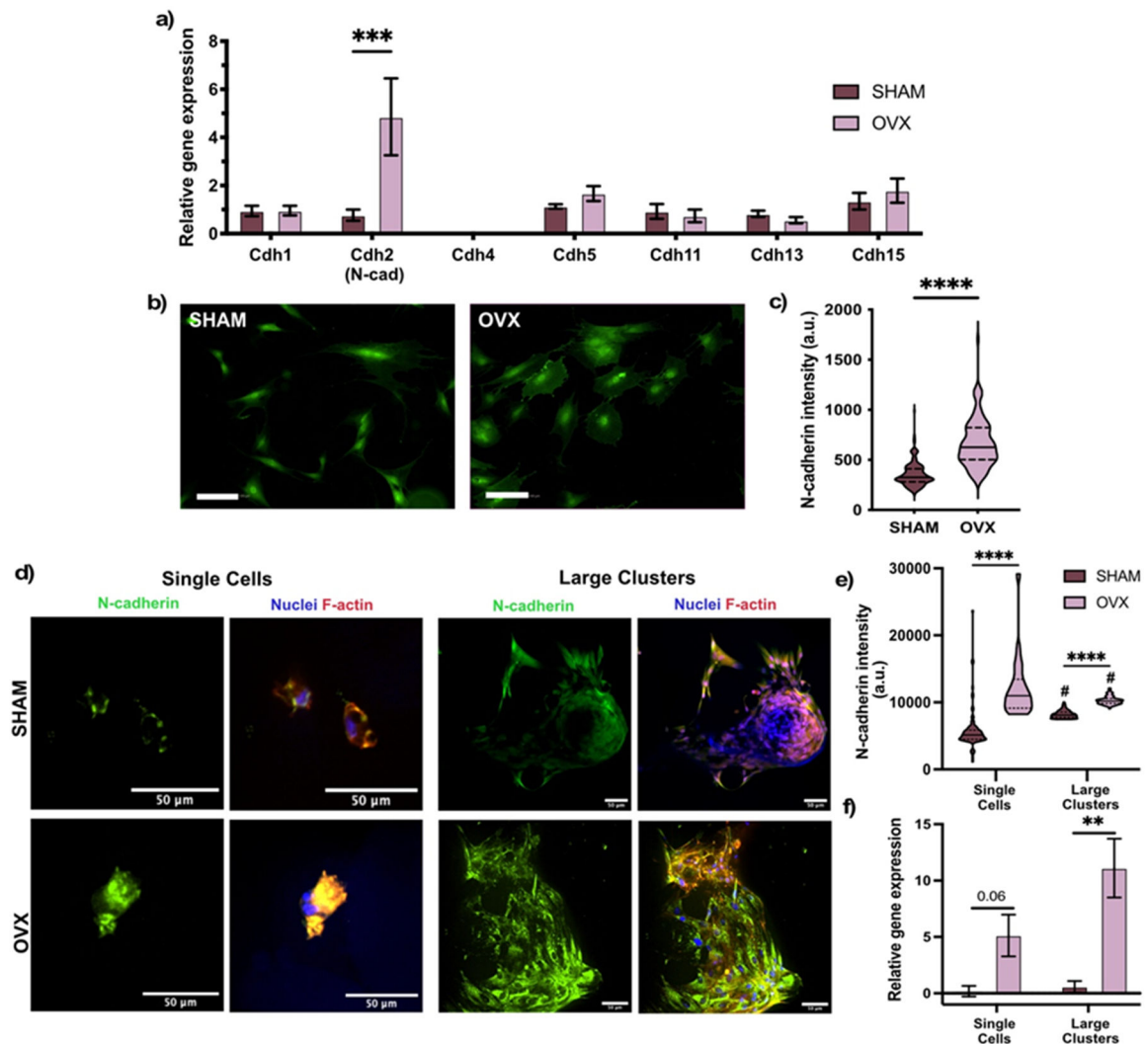
Figure 4. Higher expression of N-cadherin in OVX rMSCs.
(A) Relative expression of multiple cadherins in SHAM and OVX rMSCs cultured for 24 hours on TCPS in growth media. Error bars represent SEM. (B) Representative images of N-cadherin immunostaining (green) of SHAM and OVX rMSCs on TCPS. Scale bar (white) 100 μm. (C) Quantification of N-cadherin fluorescent intensity. Stars represent significance between OVX and SHAM (D) Representative immunostaining images of N-cadherin (green) of SHAM and OVX rMSCs cultured as single cells and as large clusters in microgel scaffolds. Nuclei are staining with DAPI (blue) and F-actin is stained with Rhodamine Phalloidin (red). (E) Quantification of N-cadherin fluorescent intensity. (F) Relative N-cadherin gene expression of SHAM and OVX rMSCs cultured in microgel scaffolds. Error bars represent SEM. Stars represent significance between SHAM (dark green) and OVX (light green) (**** p-value <0.0001, ** p-value <0.01). Hashtags represent significant between single cells and large clusters for each cell type (# p-value <0.001).
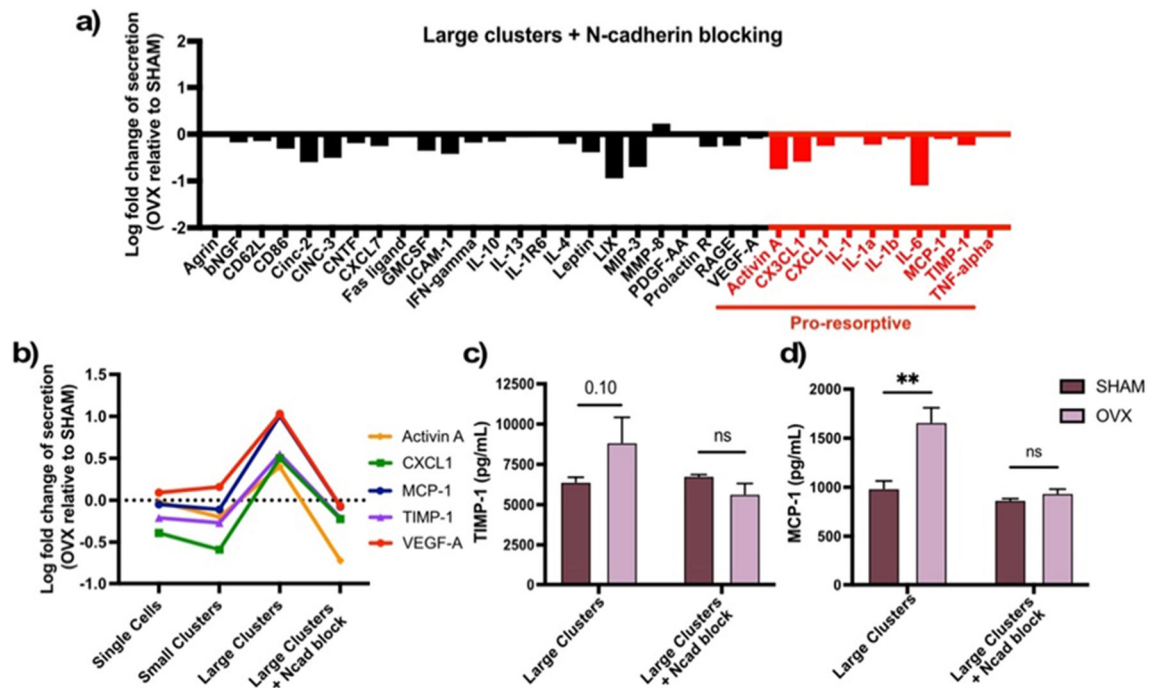
Figure 5. N-cadherin blocking decreased secretion of pro-resorptive factors selectively from OVX rMSCs.

(A) Log fold change in secretion between OVX and SHAM rMSCs cultured in large clusters with blocked N-cadherin is blocked. Pro-resorptive factors are labelled in red. (B) Log fold change of the top 5 five most elevated by OVX rMSCs in large clusters across all clustering conditions and with N-cadherin blocking. ELISA quantification of (C) TIMP-1 and (D) MCP-1 of SHAM and OVX rMSCs. Error bars represent SEM. Stars represent significance between SHAM (black) and OVX (gray) (** p-value <0.01, ns – not significant)

Table 1

List of primers for RT-qPCR genes.

Gene	Forward (5' -> 3')	Reverse (5' -> 3')	Product Length (bp)	Gene
Runx2	AAGTGGCCAGGTTCAACGAT	CAAGCTTCTGTCTGTGCCTT	171	NM_001278484.2
Bglap (osteocalcin)	ATTGTGACGAGCTAGCGGAC	TCGAGTCCTGGAGAGTAGCC	131	NM_013414.1
Pparg	CCTGTTGACCCAGAGCATGG	GGTCCACAGAGCTGATTCCG	124	NM_013124.3
Fabp4	AGAAGTGGGGAGTTGGCTTCG	ACTCTCTGACCGGATGACGA	103	NM_053365.2
Cdh1 (E-cadherin)	CCATCAACTGCCCGGAAAAT	ACCGTTGTCTCTTTGTCCCT	85	NM_031334.1
Chd2 (N-cadherin)	GGAGCCGATGAAGGAACCACA	ACCTGATCCTGACAAGCTCT	167	NM_031333.2
Chd4	CTGCGTTGATCTCCCCGAAT	TACTGCGTCCCTTTGGTGTC	88	XM_039106753.1
Chd5 (VE-cadherin)	GATGAGAATGACAACGCCCC	TTGTGTTTACTGGCACCACG	127	NM_001107407.1
Chd11 (OB-cadherin)	TTGTGAATGGGACTGGGACTG	TCACAGAGTCACAAAGCCAAA	137	NM_053392.1
Chd13 (T-cadherin)	TCAGAATGACAACCGACCCA	GGTCATCTGCATCAAACGCT	113	NM_138889.2
Chd15 (M-cadherin)	ATGAGTTCTGCTCTGCTCTTC	ACACACTGATGGGTGGGATG	160	NM_207613.1
Gapdh	GTTACCAGGGCTGCCTTCTC	GATGGTGATGGGTTTCCCGT	177	NM_017008.4